Relative Reactivity and Bioavailability of Mercury Sorbed to or Coprecipitated with Aged Iron Sulfides

Nelson A. Rivera, Jr. [§*], Paige M. Bippus[§], Heileen Hsu-Kim[§*]

[§]Department of Civil and Environmental Engineering, Box 90287, Duke University, Durham, North Carolina 27708, USA

*To whom correspondence should be addressed
nelson.rivera@duke.edu, hsukim@duke.edu

TOC Art

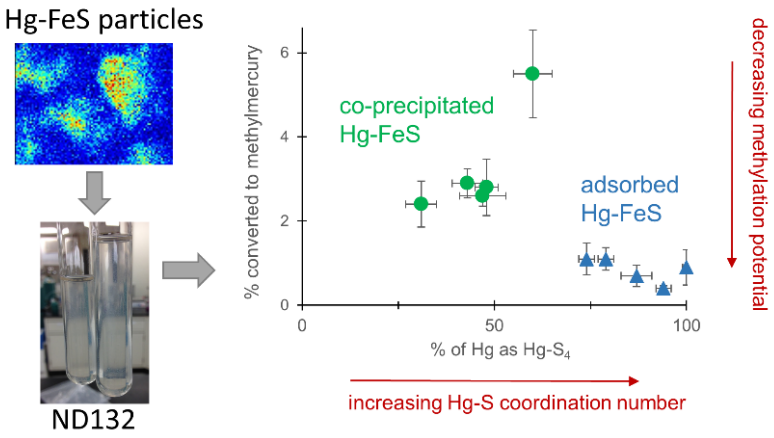

Abstract: The potential for inorganic mercury (Hg) to be converted to methylmercury depends, in part, on the chemical form of Hg and its bioavailability to anaerobic microorganisms that can methylate Hg. In anaerobic settings, Hg can be associated with sulfide phases, including ferrous iron sulfide (FeS), which can sorb or coprecipitated with Hg. The objective of this study was to determine if the aging state of FeS alters the Hg coordination environment as well as the reactivity and bioavailability of sorbed and coprecipitated Hg species. FeS particles were synthesized with and without Hg^{2+} and aged in anaerobic conditions for multiple time frames spanning from 1 hour to 1 month. For FeS particles synthesized without Hg, Hg^{2+} was subsequently sorbed to the FeS for 1 day. Analysis of Hg speciation of these materials by X-ray absorption near edge spectroscopy revealed a predominance of 4-coodinate Hg-S species in the sorbed Hg-FeS solids and a mixture of 2- and 4-coordinate Hg-S in the coprecipitated Hg-FeS. The leaching potential of the Hg was assessed by exposing the particles to a solution of dissolved glutathione (a thiolate-based Hg chelator). As expected, the sorbed Hg-FeS released more soluble Hg compared to the co-precipitated Hg-FeS. However, when these particles were exposed to *Desulfovibrio desulfuricans* ND132 (a known Hg methylator), more Hg was methylated from the co-precipitated Hg-FeS than the sorbed Hg-FeS, consistent with expectations from the Hg-S coordination state and inconsistent with the selective leaching results. Overall, these results suggest that the bioavailability of particulate Hg cannot be easily discerned by leaching potential into bulk solution. Rather, bioavailability entails more subtle interactions at particle-cell interfaces and perhaps correlates with the local Hg-S coordination state in the particles.

1. Introduction

Sulfur can play an important role in the cycling of trace metal contaminants in anaerobic environments[1, 2] by forming insoluble or sparingly soluble precipitates with sulfide. Metal sulfide mineral formation can result in long-term sequestration of trace metal contaminants in anaerobic environments. In reducing environments, iron is often important for controlling soluble sulfide speciation through the formation of iron sulfide solid phases, including the frequently observed mackinawite (FeS) [3-9]. In oxic and anoxic settings, inorganic divalent mercury Hg(II) can persist as sulfides, including polymorphs of $HgS_{(s)}$, cinnabar and metacinnabar[10-13]. Hg(II) can also associate with FeS particles (as adsorbed or coprecipitated species) in anoxic settings[3, 4, 13-17]. In the environment, the amount of iron sulfides is frequently orders of magnitude larger than the amount of mercuric sulfides in most settings, with molar ratios of Hg:FeS ranging from 1:300 to 1:300,000 in sulfidic soil and sediment settings [16, 18]. Previous laboratory studies[3, 4, 15] have demonstrated that Hg strongly sorbs to FeS, with approximately 100% Hg sorption at environmentally relevant Hg:FeS ratios and circumneutral pH. One study suggests that Hg(II) can be reduced to Hg(0) in the presence of FeS[16]; however, the precise mechanism of this process has yet to be elucidated. Note that in extremely contaminated settings (e.g., soils impacted by historical industrial point sources), the Hg:FeS ratio can exceed the range stated above. Therefore in these settings, solid phase Hg may be hosted by other mineral oxides.

The interaction of Hg(II) with FeS could be a factor limiting the bioavailability of Hg(II) to Hg-methylating microorganisms present in anoxic environments. The microorganisms that are presently known to produce methylmercury (MeHg) are all obligate anaerobes and include a subset of sulfate reducers, iron reducers, and methanogens, among others[19-25]. Microbial production of MeHg is an important first step leading to the bioaccumulation of this neurotoxin

46 in the aquatic and terrestrial food web[26]. The aging and sequestration of inorganic Hg(II) as
47 sparingly soluble or strongly bound solid phases generally limits the bioavailability of this metal
48 for methylation[27-32].

49 Given that Hg(II) is for the most part bound to solid phases in anaerobic habitats (with solid-
50 to-aqueous partition ratios typically 10^3 to 10^6)[13, 33, 34], the relative bioavailability of different
51 particulate Hg forms can be a controlling factor for MeHg levels in the environment. For
52 example, previous studies have shown that as freshly precipitated mercuric sulfide particles age
53 and aggregate, the overall bioavailability to methylating bacteria decrease with age[27, 29].
54 Nanoscale structure of HgS particles is particularly relevant in settings containing dissolved
55 organic matter (DOM), which alters the kinetics of HgS particle growth, ripening, and
56 aggregation. While many studies have reported on the role of Hg-sulfide and Hg-organic matter
57 coordination states for bioavailability to microorganisms[27, 29, 35], much less is known about the
58 role of FeS in altering Hg(II) bioavailability.

59 This study aimed to determine how the aging of the FeS precipitates affects Hg coordination
60 states and Hg bioavailability. The FeS was aged over a variety of time frames (1 hour to 1
61 month) with Hg^{2+} subsequently sorbed to the aged FeS (Hg-FeS_{ads}). Hg^{2+} was also co-
62 precipitated with the FeS for the same time frame (Hg-FeS_{ppc}). The local coordination state of
63 Hg and Fe and bulk aqueous reactivity of Hg in the resultant Hg-FeS particles were evaluated by
64 X-ray absorption spectroscopy and selective leaching. Additionally, the bioavailability of the Hg
65 was examined by exposing pure cultures of a methylating bacterium to the Hg-FeS particles and
66 quantifying the production of MeHg. The overall goal of this research was to elucidate the
67 interactions between mercury and iron sulfide (FeS) and link the structural properties of Hg-FeS
68 to bioavailability for methylating microbes.

2. Experimental Methods

2.1 Synthesis of Hg Sorbed to FeS

Iron sulfide mineral synthesis was performed in PTFE oak ridge tubes in which $Fe^{II}(NH_4)_2(SO_4)_2 \cdot 6H_2O$ and $Na_2S \cdot 9H_2O$ were both added to a final concentration of 0.1 M in 40 mL solutions adjusted to pH 4. A black precipitate formed immediately and the resultant solid was allowed to age for 1 hr, 1 day, 1 week, 2 weeks, and 1 month. Details of chemical stocks are provided in the Supporting Information (SI). All syntheses were performed inside a Coy anaerobic chamber with a nominal 97% N_2/3% H_2 gas atmosphere and a Pd catalyst for removal of trace oxygen. Both H_2 and O_2 levels in the chamber were monitored with a gas analyzer (Coy Laboratories, Model 10 Oxygen/Hydrogen Analyzer).

After the specified synthesis time, the solids were centrifuged for 20 minutes (4200 rcf) and the supernatant decanted. The solids were rinsed once with degassed deionized water to remove any excess salt. The FeS particles were then re-suspended in 40 ml of a solution of 0.3 M NaCl adjusted to pH 7, and dissolved Hg^{2+} was added to a final concentration of 1 μM (for a Hg:FeS molar ratio of 1:85,000). This aqueous Hg concentration exceeds typical values in environmental settings; however, the Hg:FeS ratio is relevant for sediments in sulfate-reducing environments. The Hg was allowed to sorb to the FeS particles for 1 day, resulting in materials that we refer to as "Hg-FeS_{ads}" for subsequent characterization, leaching and methylation experiments.

An alternate batch of FeS was later produced using the same synthesis protocol as above, except that the pH was adjusted to 7 instead of 4. These particles were aged from 1 h to 1 month, washed, and then re-suspended in 0.3 M NaCl (pH 7). Hg^{2+} was adsorbed in the same manner. The experimental results for this material are described in the SI.

2.2 Synthesis of Hg Co-precipitated with FeS

The co-precipitated Hg-FeS (referred as "Hg-FeS_{ppc}") was synthesized in a manner similar to the method in Section 2.1 except that 1 μM Hg(II) was added to the solution of 0.1 M $Fe^{II}(NH_4)_2(SO_4)_2 \cdot 6H_2O$ with a 0.3 M sodium chloride background electrolyte, prior to the addition of 0.1 M $Na_2S \cdot 9H_2O$. The sample was adjusted to pH 7 using 1 N NaOH/HCl solutions, continuously mixed end-over-end for 24 hours (except for the 1 hour sample), and then allowed to age under static conditions for time periods ranging up to 1 month. After the specified aging time, the solutions were then centrifuged and decanted. The solid phase was used (without washing) for further analysis. Portions of the supernatant aqueous phase were reserved for Hg concentration analysis.

2.3 Solid phase characterization

2.3.1 Mercury Concentrations and Mass Distribution

Total Hg contents in the Hg-FeS_{ads} - and Hg-FeS_{ppc} solids were determined by direct thermal decomposition, amalgamation, and atomic absorption spectrometry (Milestone DMA-80). A Fe_2O_3/ZnO mixture (~0.1 g per 0.05 g of Hg-FeS sample) was added to the solid prior to analysis to help quench sulfide volatilization and to prevent poisoning of the catalyst and amalgamator during decomposition of the FeS. Instrument calibrations were verified by analysis of a soil standard reference material (SRM:2709A San Joaquin sediment). The average measured value of the SRM was 0.9±0.1 mg/kg Hg (n=68), consistent with the certified value of 0.9±0.2 mg/kg Hg. Mass distribution of Hg on a Hg-FeS_{ppc} sample was assessed by synchrotron micro X-ray fluorescence spectroscopy (see SI for details).

2.3.2 X-ray Diffraction (XRD)

Major mineralogy of the FeS materials (synthesized without Hg) was evaluated by X-ray diffraction (XRD) using a Philips X'Pert Pro Diffractometer. FeS samples were mixed with 100% ethanol and dried onto Si zero background holders in an anaerobic chamber and were

analyzed immediately after drying. Diffractograms were collected from 10°-70° 2-theta with a 0.05 step size at a Cu-Kα energy (λ=1.54 Å). Although the XRD analysis was performed under atmospheric conditions, no evidence of oxidation was observed over the course of the measurement (~40 minutes).

2.3.3 X-ray Absorption Spectroscopy (XAS)

The solid phase speciation of Fe and Hg were evaluated in the Hg-FeS samples by Fe K-edge XAS (both X-ray Absorption Near Edge Spectroscopy, XANES and Extended X-ray Absorption Fine Structure, EXAFS) and Hg L_{III}-edge XANES. The Hg-FeS_{ads} and Hg-FeS_{ppc} samples (representing FeS aging states of 1 h, 1 d, 1 week, 2 weeks, and 1 month) were prepared as described in Sections 2.1 and 2.2 except with 5 μM initial Hg instead of 1 μM Hg. The increase in the initial Hg concentration was necessary as the addition of 1 μM Hg to the FeS mixtures was not enough to attain sufficient Hg XAS data quality. Although the initial Hg concentrations were greater for the XAS measurements than the Hg uptake experiments, the Hg:FeS ratios were still 1:17,000-20,000, a significant excess of FeS compared to Hg.

Both Fe and Hg XAS were collected on beamline 11-2 at the Stanford Synchrotron Radiation Lightsource (SSRL), running under dedicated conditions (3 GeV, 500 mA) using an unfocused beam. The beamline was configured with a rhodium mirror, a channel-cut Si(220) phi=90° monochromator (beam size = 1 mm vertical × 10 mm horizontal), a 100-element Ge detector, and a cut-off mirror placed in front of the first ion chamber to reject higher order harmonics. The energy scale was calibrated to the derivative maxima (11,919 eV) of an Au metal foil for Hg and of a Fe metal foil (7112 eV). Samples were mounted as wet pastes in aluminum holders with Kapton tape windows and were immediately frozen until analysis. Multiple scans

(from 6 to 9) were collected for each sample as they were held at 77 K in a liquid nitrogen cryostat.

The data collection and analysis approaches used are discussed by Kelly et al.[36]. XANES data were generally collected over three energy ranges of -200 to -50 eV, -50 to 50 eV, and 50 to 300 eV relative to the Hg or Fe edge, with smaller step sizes and larger counting times used in the region bracketing the edge (-50 to 50 eV). XANES spectra were averaged, baseline corrected with a linear model, and normalized to an edge step of 1 using the IFEFFIT suite of computer programs in the Athena and Artemis software[37]. For Hg, estimates of proportions of the species present in the samples were made using the linear combination fitting (LCF) routine in Athena to determine the combination of scaled XANES spectra from 7 reference materials[38] that gave the best-fit to sample spectra. Fitting analyses were performed over the range of 12265-12365 eV without an energy shift parameter for the calibrated data. For Fe, EXAFS was collected out to k=14 $Å^{-1}$ at a 0.05 $Å^{-1}$ step. Backgrounds were removed from EXAFS spectra using a cubic spline fit with nodes defined by the AUTOBKG function in IFEFFIT [39]. Fourier transformations of k^3-weighted spectra [$k^3*\chi(k)$] were taken across a k range of 2 to 14 $Å^{-1}$ using a Kaiser-Bessel window with a 0.5 $Å^{-1}$ sill width. The real and magnitude parts of the Fourier transformed spectra are shown in Figure S2 with a radial distance scale that is not corrected for phase shift (R + ΔR).

2.4 Hg Biomethylation Potential

A pure culture of *Desulfovibrio desulfuricans strain ND132* (ND132)[40] was grown in degassed sulfate-free pyruvate/fumarate culture media[40] to an optical density (660 nm) of 0.1 absorbance units, corresponding to approximately 2×10^7 cells mL^{-1}.[41] The cultures were then split into glass hungate tubes in 10-ml aliquots and the Hg-FeS_{ads} and Hg-FeS_{ppc} solids were

added (to final concentrations corresponding to 3-5 μg/L Hg and ~176 mg/L FeS). Samples were rotated continuously end-over-end in the dark for 5 hours, and then preserved with 0.5% HCl and frozen until total Hg and MeHg analysis.

Experimental controls included the following: 1) Killed control comprising bacterial cultures inactivated by autoclaving and then amended with 5 μg/L dissolved Hg(II) from an acidified Hg^{2+} stock solution; 2) Abiotic control comprising sterile culture media amended with 5 μg/L Hg^{2+}; 3) Positive control comprising the ND132 culture amended with 5 μg/L Hg^{2+}; 4) Methylmercury (from a dissolved CH_3HgCl stock solution) added to the microbial culture ascertain biological demethylation; and 5) Methylmercury to an abiotic FeS solution (176 mg/L, 1 day old) to ascertain abiotic demethylation. All methylation experiments and controls were performed in triplicate and in an anaerobic chamber.

Samples reserved for MeHg analysis were thawed and spiked with an isotopically-enriched $Me^{201}Hg$ stock solution as an internal standard[42-44]. The samples (5 mL) were then amended with 200 μL of 20% KCl, 1000 μL 9M H_2SO_4, and 2 mL of 1 M $CuSO_4$, brought to a final volume of 25 ml with 18.2 MΩ DI water and then heated at 125 °C for the MeHg distillation process[45, 46]. MeHg concentrations in the distillates were determined by aqueous phase ethylation, purging onto a Tenax resin with gas chromatographic separation, and analysis by inductively coupled plasma mass spectrometry[45] (Brooks Rand, Merx-M, Agilent 7700). The reported MeHg concentration for each sample was corrected by the recovery of $Me^{201}Hg$ internal standard (which ranged from 35 to 95%). A SRM (IAEA-086, human hair) was included for each distillation batch. The average measured value of the SRM was 0.237±0.011 mg MeHg/kg solid (n=6), consistent with the certified value of 0.258±0.022 mg MeHg/kg solid.

2.5 Hg Reactivity by Selective Leaching

The leaching potential of Hg associated with the Hg-FeS_{ads} and Hg-FeS_{ppc} samples was tested by suspending the solids (corresponding to 3-5 μg/L Hg) in sterilized degassed culture media with or without 1 mM glutathione (GSH), a water soluble Hg^{2+}-chelating ligand. The use of GSH was based on selective extraction procedures described previously[47]. The addition of GSH to a suspension of FeS particles may result in the loss of GSH from solution (via sorption to FeS or oxidation of GSH). Nevertheless, this leaching process was used as a potential measure of Hg reactivity relevant to the leaching of Hg in the presence of a thiolated biotic ligand at the particle-bacterial cell interface.

All leaching experiments were performed in triplicate and prepared in an anaerobic chamber. The extraction was performed for 1 hour, then centrifuged outside the anaerobic chamber at 4200 rcf for 10 minutes, and then the supernatant was filtered using a 0.22 micron polyethersulfone filter. The supernatant was diluted with ultrapure water to a 20 ml final volume and acidified with 2% (v/v) BrCl before total dissolved Hg analysis. Total mercury was analyzed by stannous chloride reduction, gold amalgamation, and cold vapor atomic fluorescence spectroscopy (Brooks Rand, Merx-T)[48].

2.6 Data Analyses

Analysis results of experimental triplicates are reported as mean ± standard deviation. The non-parametric Mann-Whitney U test was used to test the following null hypotheses: 1) for each type of material, the percentages Hg leached are the same in culture media+GSH and in media without GSH; 2) %Hg leached in media+GSH are the same for Hg-FeS_{ads} and Hg-FeS_{ppc} sample groups; 3) % methylation values are the same for Hg-FeS_{ads} and Hg-FeS_{ppc} sample groups. Significant differences were defined at $p<0.05$.

3.0 Results

3.1 Major Mineralogy and Fe Coordination Environment of the Hg-FeS particles

Both XRD and Fe-EXAFS analysis of the synthesis of iron sulfide demonstrated that the materials were predominantly in the form of mackinawite (FeS). The XRD spectra for the synthesized material at pH 4 (Figure S1) showed a major peak intensity at ~17° 2-theta consistent with mackinawite formation for samples aged from 2 hours to 30 days. Crystallite size analysis by the Scherrer equation[49] showed an increase in crystallite size from 8 nm at 2 hours to 28 nm at 30 days. No other phases were evident in the XRD spectra besides the residual salt peaks. A new peak appeared after 30 days corresponding to pyrite (100% line at 33°) and an increase in the peak intensity at 30° (greigite peak 100% line) relative to the mackinawite at 17°, suggesting the formation of secondary iron sulfide phases. For this reason, we did not utilize FeS aging states beyond 30 days for the Hg experiments. There was no evidence of iron oxide phases over the course of the synthesis time nor iron oxide formation during the XRD measurement.

Iron K-edge XANES and EXAFS data of the sorbed and co-precipitated Hg-FeS samples also indicated mackinawite-like FeS structures (Figure S2). The Fe-XANES spectra (Figure S2A) have a pre-edge feature at 7112 eV and a second edge feature at 7120 eV that matched the reference FeS spectra. The k^3-weighted EXAFS data (Figure S2B) for all Hg-FeS samples demonstrated similar spectral features at k=7.5 $Å^{-1}$ and 8.5-10.5 $Å^{-1}$ compared to the FeS mackinawite reference. Also, Fourier transforms of the Hg-FeS_{ads} and Hg-FeS_{ppc} spectra comprised two distinct peaks at 2.26 Å and 2.60 Å, consistent with first- and second-shell Fe coordination states of mackinawite[16, 50, 51]. The differences in pH during FeS synthesis may have contributed to small variations in local Fe coordination. (Hg-FeS_{ppc} was synthesized at pH 7, while the FeS without Hg was synthesized at pH 4, but then sorbed with Hg at pH 7). Regardless, the data collectively indicated that the Fe was in the form of mackinawite FeS in

232 both the Hg-FeS_{ads} and Hg-FeS_{ppc} materials with no evidence of secondary phases such as pyrite
233 or greigite nor evidence of oxidation.

234 While Fe speciation was similar between the sorbed and co-precipitated Hg-FeS samples,
235 major differences were observed in terms of Hg content and reactivity. For example, the amount
236 of Hg associated with the iron sulfide particles (relative to the Hg added) depended on the
237 method of Hg addition (Figure 1). For the Hg-FeS_{ads} particles, approximately 100% of the Hg
238 added to the FeS suspension was measured on the particles. The total Hg contents in these solid
239 phases were ~29-34 μg/g for Hg-FeS_{ads} and the amount of solids produced was ~0.25 grams. Hg
240 concentration in the supernatants of the Hg-FeS mixtures was less than 1 μg/L, or less than 0.5%
241 of added Hg.

242 For the co-precipitated materials (Hg-FeS_{ppc}), only 60% ± 5% of the added Hg was
243 measured on the solid phase after 1 hour of precipitation time (Figure 1). This percentage
244 increased to 80% ± 12% after 30 days of co-precipitation. The solid phase Hg content ranged
245 from 13 to 18 μg per g of Hg-FeS_{ppc} (μmol Hg per mol FeS), and the amount of solids produced
246 was ~0.35 grams. Hg concentrations in the supernatant solutions of the Hg-FeS_{ppc} (for all aging
247 states) were all less than 1% of the added Hg. Unfortunately Hg contents in the headspace of the
248 reaction vessels were not sampled for measurements to close mass balance.

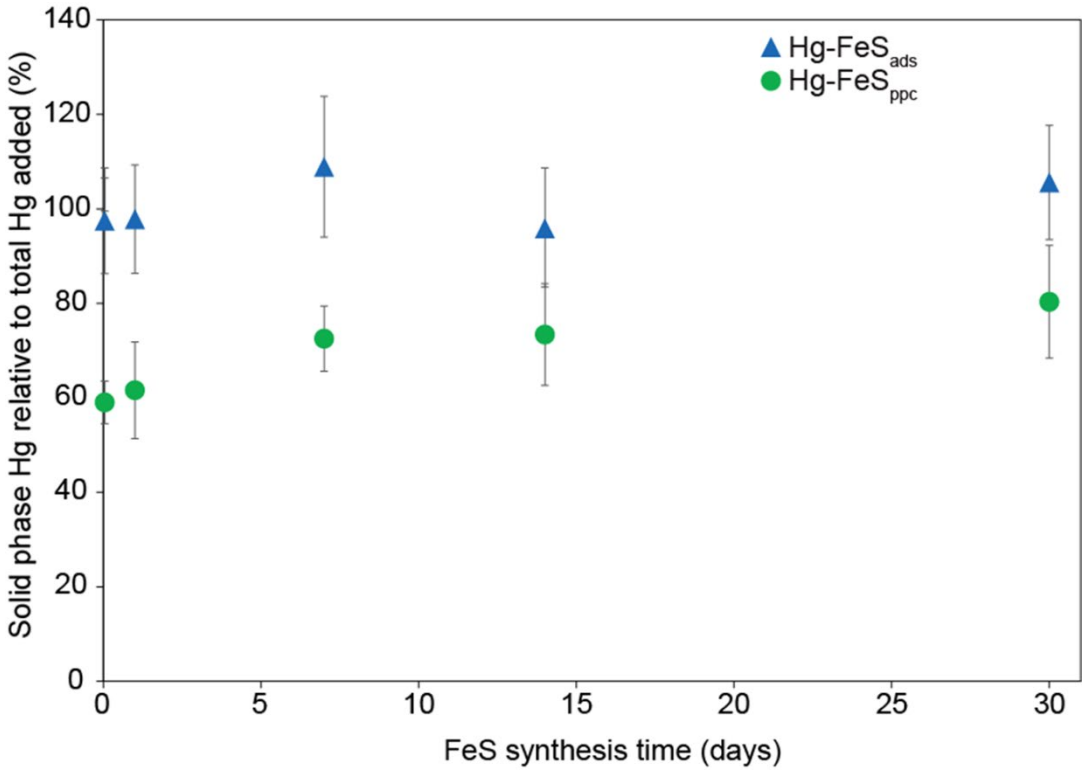

Figure 1. The measured solid phase Hg relative to the total Hg added to suspensions of pre-synthesized FeS (for Hg-FeS$_{ads}$) or the suspensions of FeS forming in the presence of Hg (Hg-FeS$_{ppc}$). Data points correspond to the average (±1 standard deviation) of triplicate samples.

3.2 Relative Bioavailability of Sorbed and Co-precipitated Hg-FeS

The bioavailability and methylation potential of Hg-FeS particles differed between the sorbed and co-precipitated forms and depended less on the aging time frame. After 5 hours exposure to the ND132 culture, approximately 1% of the added Hg from the Hg-FeS$_{ads}$ particles was converted to MeHg, regardless of the FeS aging state (Figure 2). Note that these percentages are normalized to the total Hg content measured on the Hg-FeS$_{ads}$ and Hg-FeS$_{ppc}$ particles after their synthesis and added to the cultures.

In the cultures amended with Hg-FeS$_{ppc}$ particles, significantly ($p<0.05$) larger percentages of the added Hg (relative to the Hg-FeS$_{ads}$) was methylated during the biomethylation experiment (Figure 2). Approximately 6% of the added Hg was converted to

MeHg for the 1 h-old Hg-FeS_{ppc} particles, and approximately 2% to 3% of the added Hg was methylated for the older Hg-FeS_{ppc} particles (1 d to 1 month old).

The killed control and abiotic controls that were spiked with Hg^{2+} were observed to have less than 0.1% as MeHg after 5 hours of incubation, confirming that MeHg concentrations in the Hg-FeS exposure experiments were the result of a biological process (Figure S5B). The positive control (e.g., ND132 culture amended with dissolved Hg^{2+}) resulted in 25% conversion to MeHg after 5 h, indicating an upper range of expected methylation potential for this time period and growth conditions (Figure S5B). Degradation of MeHg was not observed in cultures amended with dissolved MeHg or in sterile culture media amended with FeS particles and MeHg (Figure S5C).

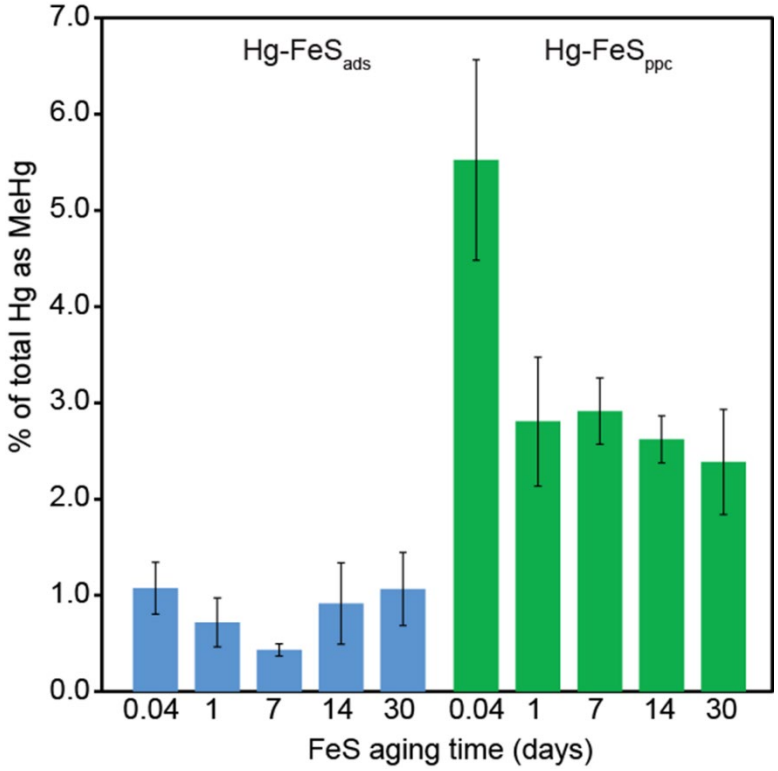

Figure 2. Percent conversion to methylmercury (MeHg) when ND132 was exposed for 5 hours to sorbed and coprecipitated Hg-FeS, synthesized at different FeS aging periods. The bars and error bars represent the average ± 1 standard deviation of triplicate cultures.

3.3 Desorption and Extractability of Hg from Hg-FeS Particles

The biomethylation experiments indicated that the relative bioavailability and methylation potential of Hg initially bound to FeS depended on its mode of synthesis (e.g., sorbed to or co-precipitated with FeS). Therefore, selective leaching studies in sterile culture media and media spiked with glutathione were performed to assess the dissolution/desorption potential of Hg associated with the Hg-FeS solids. The desorption or dissolution of Hg in the un-amended culture media resulted in relatively small percentages of soluble Hg after both the sorbed and coprecipitated Hg-FeS forms were added to the culture media (Figure 3A). For both sets of solids, <0.3% of the total Hg was leached. The 0.04- and 1-day Hg-FeS_{ppc} samples exhibited the most leaching.

In the presence of glutathione (Figure 3B), more Hg leached into solution compared to the experiment with no GSH ($p<0.05$) (Figure 3A). The GSH-extractable Hg fraction was 1.2-2.4% for the Hg-FeS_{ads} samples with large variability observed for triplicate extractions. In contrast, the Hg- FeS_{ppc} GSH extractable fraction was 0.2-0.4%,lower than the extractable fraction of the adsorbed Hg-FeS ($p<0.05$).

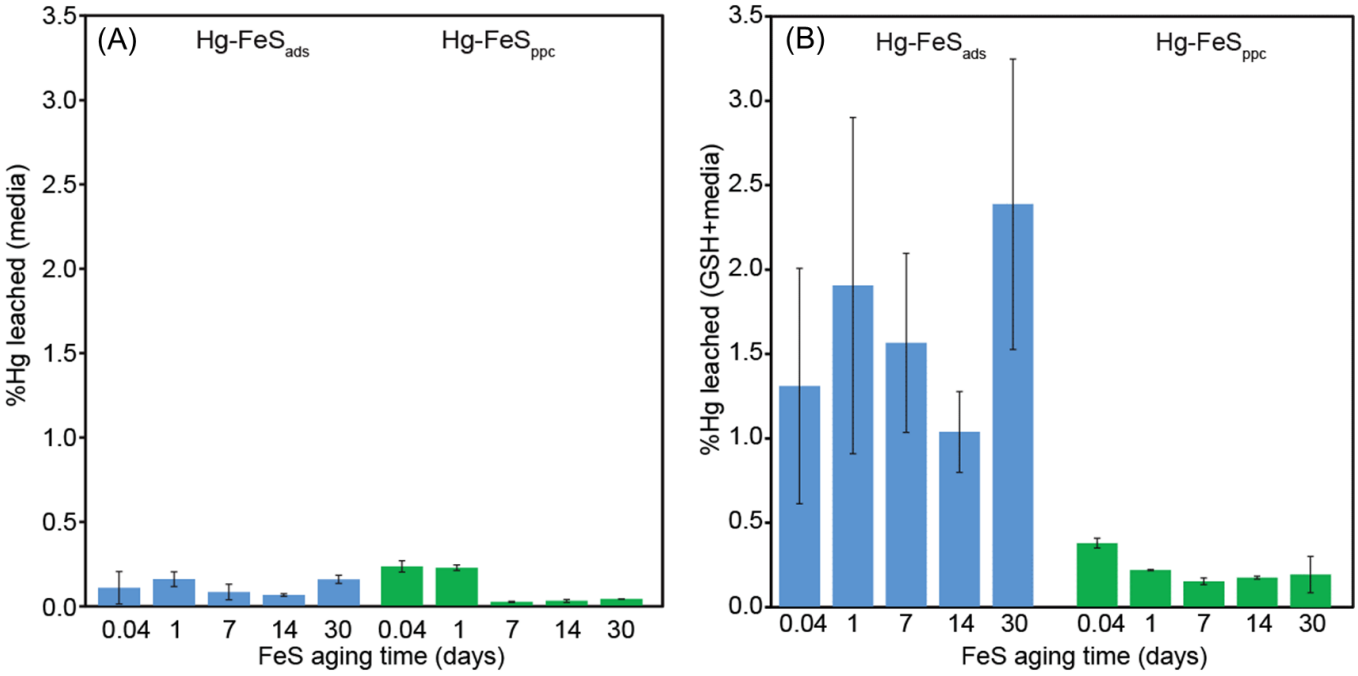

296

297 **Figure 3.** (A) The percentage of soluble Hg (i.e. 0.2 µm filter passing fraction) after Hg-FeS$_{ads}$
298 and Hg-FeS$_{ppc}$ were suspended in sterile culture media for 1 h. (B) The percentage leached in
299 culture media containing 1 mM glutathione (i.e. the GSH-extractable fraction) Bars represent
300 the average (±1 standard deviation) of triplicate samples.

301

302 **3.4 Short Range Hg Coordination State in Hg-FeS Particles**

303 The analysis of Hg coordination states for the Hg-FeS solids revealed subtle differences
304 between the Hg-FeS$_{ads}$ and Hg-FeS$_{ppc}$ in the Hg L$_3$-edge XANES spectra (Figure 4). These
305 differences were more apparent in the LCF model results (Table 1). The metacinnabar reference
306 spectra was dominant in the fits (74-100%) for the Hg-FeS$_{ads}$ spectra. Note that the analysis of
307 the local Hg coordination state via XANES does not necessarily suggest discrete Hg phases,
308 which were not observed in micro X-ray fluorescence maps (Figure S8). Rather, we interpret
309 this to indicate the predominance of tetrahedral coordination of Hg (e.g. Hg-S$_4$) that is the
310 characteristic Hg coordination environment of metacinnabar. The corderoite (Hg$_3$S$_2$Cl$_2$)
311 reference spectra accounted for a minor component (0-26%) of the fits. The local Hg bonding
312 environment of corderoite comprises a S-Hg-S bond (2.45 Å and 166.6°) and a Cl-Hg-Cl bond

(2.87 Å and 108.9°)[52]. Thus, we interpret this minor component to signify fewer than 4 S atoms per Hg (e.g., linear-type Hg-S_2 coordination). As the FeS aging state increased from 1 h to 2 weeks, the proportion of the corderoite phase decreased from 21% to 0% of the spectral fits and then increased to 26% for the 1 month sample. Note that Hg sorption time to FeS was constant (24 h) for all aging states of FeS.

Spectra for the co-precipitate Hg-FeS_{ppc} samples were fit with smaller proportion of the metacinnabar reference (40-57%) and larger percentage (summing to 40-69%) of corderoite and cinnabar. Cinnabar is a HgS polymorph with linear Hg-S_2 coordination. These fitting results suggest that the short range coordination state of Hg in Hg-FeS_{ppc} resembled a smaller proportion of tetrahedral-type Hg-S_4 coordination and larger proportion of linear-type Hg-S_2 coordination compared to the Hg-FeS_{ads}. The four-coordinate metacinnabar-like phase decreased from 1 hour to 1 month of aging time for the Hg-FeS_{ppc}, a trend that was not observed for the Hg-FeS_{ads} samples.

Measureable differences were also observed when composite spectra of the Hg-FeS_{ppc} samples were compared to the composite spectra of the Hg-FeS_{ads} samples (Figure S9). Notably, a difference of approximately 6 eV was observed on the peak shoulder near the 12290-12310 eV energy range. This comparison further suggests dissimilarities in Hg coordination between the co-precipitated and adsorbed Hg-FeS.

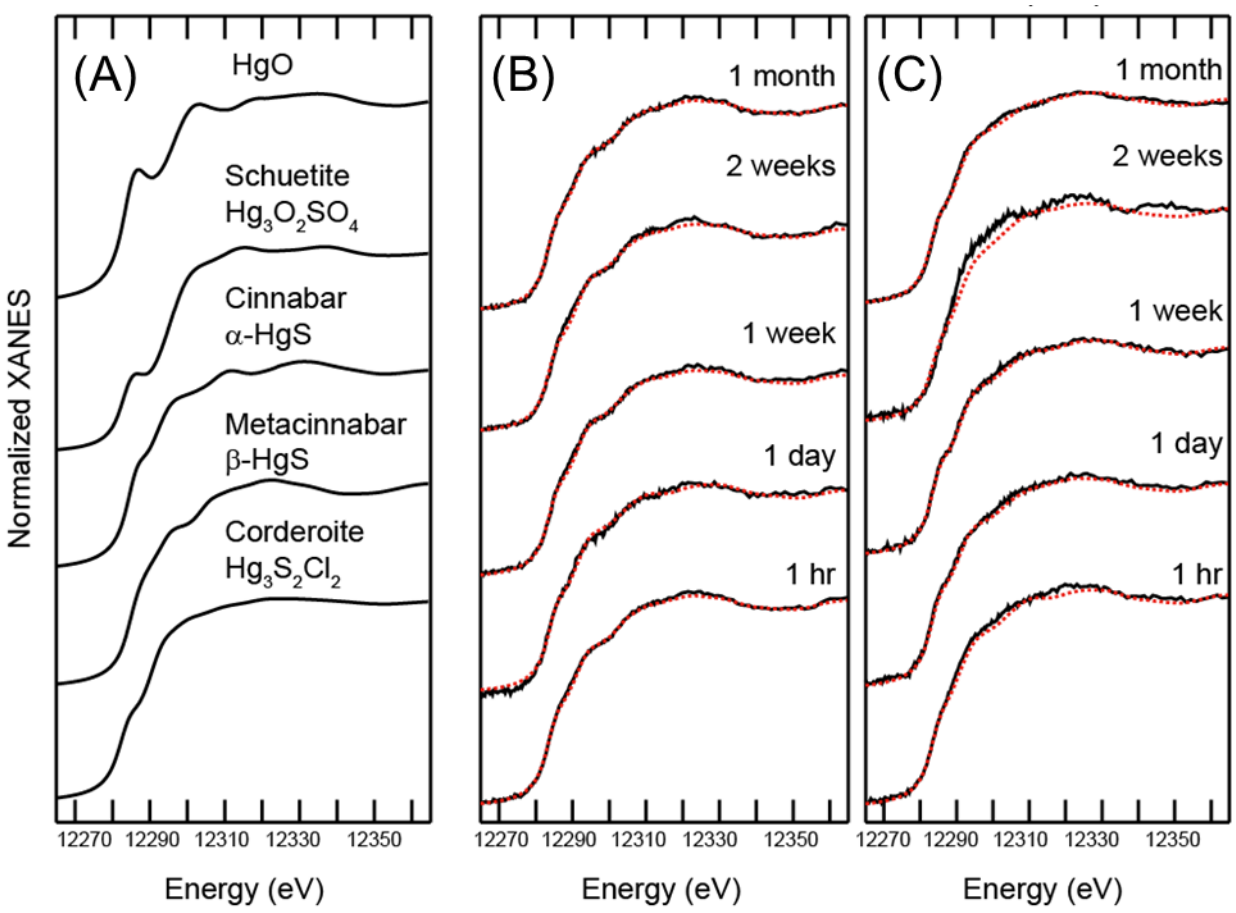

Figure 4. Hg L3-edge X-ray Absorption Near Edge spectra (solid black lines) of (A)) Hg reference materials, (B) Hg-FeS_{ads} , and (C) Hg-FeS_{ppc}. The sample spectra were modeled through linear combination fitting of the reference spectra (dotted red lines) and model results are shown in Table 1.

Table 1. Results of linear combination fitting (LCF) showing % of reference spectra (fit) (± uncertainty) for the model fit of Hg-XANES spectra (data) for the sorbed Hg-FeS_{ads} or coprecipitated Hg-FeS_{ppc}. The time points correspond to FeS age. For Hg-FeS_{ads}, Hg was sorbed to aged FeS particles for 24 hours. For the Hg-FeS_{ppc} samples, Hg and Fe were aged together in sulfide solution. The fitting range of each spectrum was 12265 eV to 12375 eV. The sum of the individual components was fixed at 100%. Without this constraint, the sum of the fittings ranged from 99-104%.

	Hg-XANES Individual components (%)			
Sample	**corderoite $Hg_3S_2Cl_2$**	**metacinnabar β-HgS**	**cinnabar α-HgS**	**R-factor[a]**
Hg-FeS$_{ads}$				
1 hour	21 ± 2	79 ± 2		0.001
1 day	13 ± 4	87 ± 4		0.003
1 week	6 ± 2	94 ± 2		0.001
2 weeks		100 ± 1		0.001
1 month	26 ± 2	74 ± 2		0.001
Hg-FeS$_{ppc}$				
1 hour	40± 5	60 ± 5		0.002
1 day	52± 5	48 ± 3		0.002
1 week	26± 5	43 ± 4	31± 7	0.001
2 weeks	53± 6	47 ± 6		0.006
1 month	51± 4	31 ± 4	18± 6	0.001

[a]R-factor = $\sum(\text{data} - \text{fit})^2 / \sum(\text{data})^2$

4.0 Discussion

The sorption, coordination state, and methylation potential of Hg differed between the two types of FeS solids (Hg-FeS_{ads} and Hg-FeS_{ppc}) synthesized in this study. In the synthesis of the Hg-FeS particles, the contents of Fe and S were much greater than Hg content (Hg:FeS_{ads} = 1:85000, Hg:FeS_{ppc} = 1:130000 mole ratio). We also observed full recovery of added Hg during the synthesis of Hg-FeS_{ads}. However, in the synthesis of Hg-FeS_{ppc}, the added Hg was incompletely recovered. This low recovery was possibly due to the conversion of Hg(II) to Hg^0 by FeS or aqueous Fe (II) (as seen in other studies[16, 53, 54]), a process that could facilitate gaseous evasion of Hg from solution during centrifugation and separation. The increase of Hg associated with the solid phase after 30 days could indicate re-oxidation of Hg and association with the Hg-

368 FeS solids. Unfortunately, measurements of the container headspace were not performed to
369 confirm this loss mechanism.
370 Mercury XANES data indicated structural differences of Hg associated with the two
371 types of Hg-FeS solids even though the Fe speciation was very similar between them. The Hg-
372 FeS_{ppc} exhibited greater proportion of linear-type Hg-S_2 coordination while the Hg-FeS_{ads} solid
373 phase was dominated by tetrahedral Hg-S_4 coordination. Our observation of both linear and
374 tetrahedral local coordination environments was consistent with previous studies of synthesized
375 Hg-FeS solids[4, 15-17]. Collectively, these previous works indicated that materials containing high
376 Hg:FeS ratio (1:22) generally comprised tetrahedral-like Hg-S coordination while materials of
377 lower Hg:FeS ratio (1:5000) resulted in linear-like Hg-S coordination. However, in this previous
378 work, the incorporation mechanism of Hg on the solids (i.e. sorption vs co-precipitation) was not
379 compared. Our Hg-FeS_{ads} and Hg-FeS_{ppc} were synthesized on the lower end of the molar ratio
380 range (Hg:FeS_{ads} = 1:85000, Hg:FeS_{ppc} = 1:130000) and closer to conditions observed in typical
381 sulfidic soils and sediments with diffuse inputs of Hg[16]. Moreover, our study provides new data
382 demonstrating that both types of Hg-S coordination environments are possible and depend on the
383 mode of incorporation (sorption or co-precipitation) as well as aging state.
384 The evolution of Hg-S coordination in the co-precipitated material did not follow a
385 pattern consistent with pure HgS formation. Previous XAS studies on metacinnabar formation
386 and HgS formation in the presence of dissolved organic matter reported that Hg initially
387 developed linear two-coordinate Hg-S_2 species that evolved to tetrahedral Hg-S_4 forms[17, 29, 55, 56].
388 This pattern is the opposite of our observations for Hg-FeS_{ppc}. While the differences in Hg and
389 sulfide concentrations are potential factors that contribute to disparities between studies, the
390 comparison also highlights major mechanistic differences of precipitation and aging of pure HgS

391 and HgS-DOM mixtures as compared to Hg-FeS mixtures. It is possible that the formation of
392 FeS hinders the aggregation of the HgS, preventing the linear HgS clusters from evolving into a
393 tetrahedrally coordinated Hg-S configuration.

394 The bioavailability and methylation potential of the coprecipitated form (Hg-FeS_{ppc}) was
395 notably greater than the methylation potential of the adsorbed material Hg-$FeS_{ads.}$ A difference
396 between Hg-FeS_{ppc} and Hg-FeS_{ads} is the pH for FeS synthesis. FeS was synthesized at pH 4 for
397 the Hg-FeS_{ads} and the Hg^{2+} sorption step occurred at pH 7, while Hg-FeS_{ppc} was synthesized at
398 pH 7. Changes in pH conditions of the FeS synthesis could result in variations in the specific
399 surface area of the solids, which we did not attempt to quantify due to potential artifacts
400 introduced by drying the particles for the analysis[6, 57]. The potential difference in specific surface
401 area between the two syntheses could lead to changes in the number of reactive surface sites
402 available for the FeS at pH 4 and 7. To address this discrepancy, we synthesized another batch of
403 FeS at pH 7, and then washed and sorbed Hg^{2+} using the same method as Hg-FeS_{ads} (Figure S4).
404 The extent of Hg methylation for this material (herein referred as "Hg-FeS_{ads_B}") was similar to
405 Hg-FeS_{ads} ($p=0.23$) and also less than Hg-FeS_{ppc} ($p<0.001$) (Figure S5A). The Fe EXAFS of Hg-
406 FeS_{ads_B} was similar to Hg-FeS_{ppc} and Hg-FeS_{ads} (Figure S2B). Hg-XANES data for Hg-FeS_{ads_B}
407 is unfortunately not available. Overall, these results suggest that for the biomethylation potential
408 of our Hg-FeS materials, the mode of Hg incorporation into the FeS was more important than
409 short-range Fe coordination state.

410 Methylation potential appeared to coincide with trends in mercury-sulfur coordination
411 states: methylation potential decreased with increased abundance of tetrahedral Hg-S_4
412 coordination (Figure 5A). Altogether, the patterns in methylation potential are counter to the
413 notion that surface bound Hg (e.g., adsorbed) is more readily bioavailable than Hg atoms

414 entrapped in a FeS matrix, as demonstrated by the GSH selective leaching data versus %
415 methylation (Figure 5B,C). This understanding of the distribution of Hg on the FeS particles
416 might be an oversimplification, though, as the Hg-coordination state might be a better indicator
417 of bioavailability. The same general trend was observed in a previous study comparing various
418 aging states of HgS particles formed in the presence of humic acid[29]. While results of this and
419 previous studies involved polynuclear phases of Hg(II)-sulfides, one could reasonably
420 hypothesize similar structure-activity relationship for Hg-organic matter compounds. Hg^{2+} ions
421 sorbed to or complexed by natural organic matter can be singly or doubly coordinated to thiolate
422 moieties[58-60], and future work could compare the methylation potential of Hg across a range of
423 Hg-S coordination states.
424 The difference in the methylation of coprecipitated and adsorbed Hg-FeS forms was
425 notably inconsistent with expectations of the GSH leaching results, which demonstrated greater
426 leaching from Hg-FeS_{ads} than from Hg-FeS_{ppc}. In previous work with Hg isotope spikes in
427 sediment slurries, GSH-leachable concentrations and Hg methylation potential correlated in a
428 freshwater slurry culture but did not correlate in a mesohaline slurry culture.[61] As noted in that
429 study, certain sample matrices may be vulnerable to changes during the sampling handling of the
430 GSH extraction (i.e. centrifugation steps and temporary exposure to oxygen). The results here
431 further demonstrate uncertainties with the GSH-extractable fraction as a measure of Hg
432 bioavailability in sediment cultures.

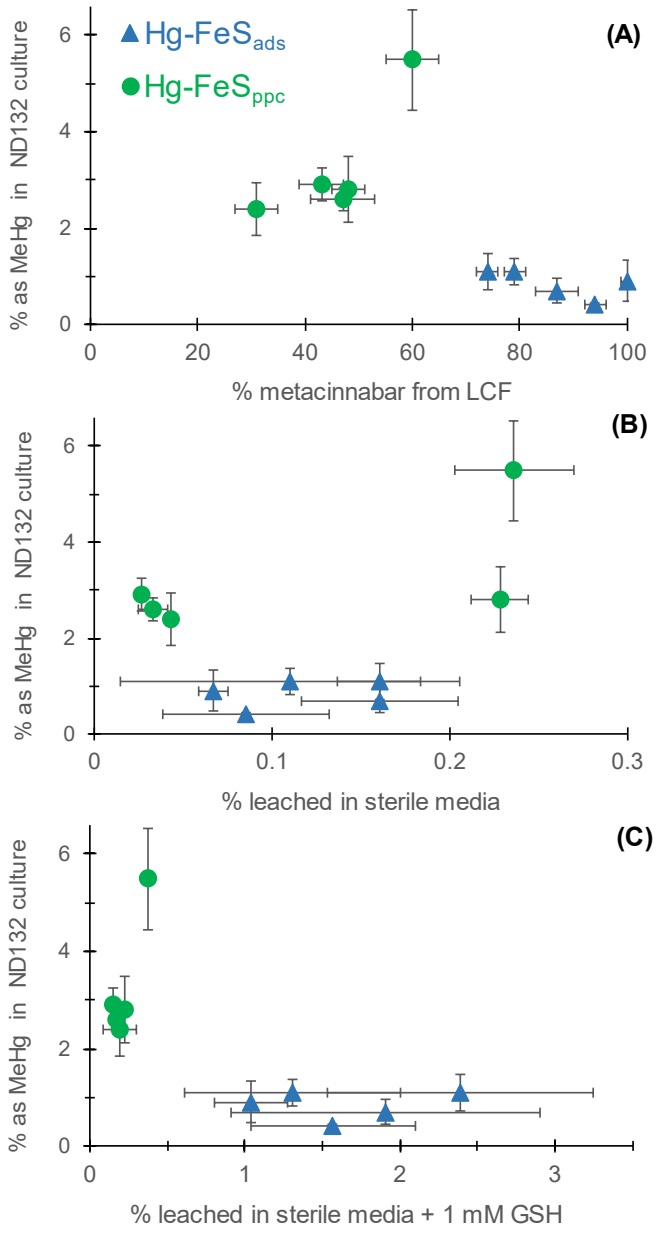

433

434 **Figure 5.** The percentage of added Hg-FeS_{ads} and Hg-FeS_{ppc} converted to methylmercury
435 (MeHg) by ND132 plotted as a function of: (A) % as metacinnabar HgS by linear combination
436 fitting of XANES spectra for various aging states of each material; (B) % leached after 1 hour in
437 sterile culture media; (C) % leached after 1 hour in sterile culture media containing 1 mM GSH.
438

439 **Environmental Implications**

440 The fate and transport of mercury in the environment can be controlled by a variety of

441 factors including aqueous sulfide concentrations, dissolved ferrous iron, and sequestration by

secondary mineral formation with iron sulfides[18, 62-65]. Anaerobic environments with high sulfate and dissolved iron inputs have been shown to decrease methylation rates, either due to aqueous Hg complexation with (bi)sulfide, precipitation of mercuric sulfide species, or reactions with iron sulfide phases. Here, we showed that molecular-level changes of Hg-FeS forms could influence methylation potential of the metal. The aging time of FeS beyond 1 day as well as dissolution/desorption potential of Hg into bulk solution were notably less important for Hg methylation than the local Hg coordination environment. These insights might guide future efforts to improve methods for quantifying Hg bioavailability and biomethylation potential in complex environmental mixtures.

Supporting Information: Additional details on materials, micro X-ray fluorescence methods and results, additional microbial methylation data.

Acknowledgements

This study was supported by the Department of Energy (DE-SC0006938, DE-SC0019408), the National Institute of Environmental Health Sciences Superfund Research Program (R01ES24344), and the Center for Environmental Implications of NanoTechnology supported by the National Science Foundation and the Environmental Protection Agency (DBI-1266252). Use of the Stanford Synchrotron Radiation Lightsource, SLAC National Accelerator Laboratory, is supported by the U.S. Department of Energy, Office of Science, Office of Basic Energy Sciences under Contract No. DE-AC02-76SF00515. We thank C. Gilmour and A. Soren at the Smithsonian Environmental Research Center for the ND132 culture and their advice on this work.

References

1. Yang, Y.; Chen, T. H.; Sumona, M.; Sen Gupta, B.; Sun, Y. B.; Hu, Z. H.; Zhan, X. M., Utilization of iron sulfides for wastewater treatment: a critical review. *Reviews in Environmental Science and Bio-Technology* **2017,** *16*, (2), 289-308.
2. Julian, P.; Chambers, R.; Russell, T., Iron and Pyritization in Wetland Soils of the Florida Coastal Everglades. *Estuaries and Coasts* **2017,** *40*, (3), 822-831.
3. Jeong, H. Y.; Klaue, B.; Blum, J. D.; Hayes, K. F., Sorption of Mercuric Ion by Synthetic Nanocrystalline Mackinawite (FeS). *Environmental Science & Technology* **2007,** *41*, (22), 7699-7705.
4. Jeong, H. Y.; Sun, K.; Hayes, K. F., Microscopic and Spectroscopic Characterization of Hg(II) Immobilization by Mackinawite (FeS). *Environmental Science & Technology* **2010,** *44*, (19), 7476-7483.

5. Csákberényi-Malasics, D.; Rodriguez-Blanco, J. D.; Kis, V. K.; Rečnik, A.; Benning, L. G.; Pósfai, M., Structural properties and transformations of precipitated FeS. *Chemical Geology* **2012,** *294-295*, 249-258.
6. He, Y. T.; Wilson, J. T.; Wilkin, R. T., Impact of iron sulfide transformation on trichloroethylene degradation. *Geochimica et Cosmochimica Acta* **2010,** *74*, (7), 2025-2039.
7. Rickard, D.; Luther, G. W., Chemistry of Iron Sulfides. *Chemical Reviews* **2007,** *107*, (2), 514-562.
8. Thiel, J.; Byrne, J. M.; Kappler, A.; Schink, B.; Pester, M., Pyrite formation from FeS and H₂S is mediated through microbial redox activity. *Proceedings of the National Academy of Sciences* **2019,** *116*, (14), 6897.
9. Rickard, D.; Mussmann, M.; Steadman, J. A., Sedimentary Sulfides. *Elements* **2017,** *13*, (2), 117-122.
10. Benoit, J. M.; Gilmour, C. C.; Mason, R. P.; Heyes, A., Sulfide Controls on Mercury Speciation and Bioavailability to Methylating Bacteria in Sediment Pore Waters. *Environmental Science & Technology* **1999,** *33*, (6), 951-957.
11. Hsu-Kim, H.; Sedlak, D. L., Similarities between Inorganic Sulfide and the Strong Hg(II)-Complexing Ligands in Municipal Wastewater Effluent. *Environmental Science & Technology* **2005,** *39*, (11), 4035-4041.
12. Manceau, A.; Lemouchi, C.; Enescu, M.; Gaillot, A.-C.; Lanson, M.; Magnin, V.; Glatzel, P.; Poulin, B. A.; Ryan, J. N.; Aiken, G. R.; Gautier-Luneau, I.; Nagy, K. L., Formation of Mercury Sulfide from Hg(II)–Thiolate Complexes in Natural Organic Matter. *Environmental Science & Technology* **2015,** *49*, (16), 9787-9796.
13. Liem-Nguyen, V.; Skyllberg, U.; Björn, E., Thermodynamic Modeling of the Solubility and Chemical Speciation of Mercury and Methylmercury Driven by Organic Thiols and Micromolar Sulfide Concentrations in Boreal Wetland Soils. *Environmental Science & Technology* **2017,** *51*, (7), 3678-3686.
14. Liu, J.; Valsaraj, K. T.; Devai, I.; DeLaune, R. D., Immobilization of aqueous Hg(II) by mackinawite (FeS). *Journal of Hazardous Materials* **2008,** *157*, (2), 432-440.
15. Skyllberg, U.; Drott, A., Competition between Disordered Iron Sulfide and Natural Organic Matter Associated Thiols for Mercury(II)—An EXAFS Study. *Environmental Science & Technology* **2010,** *44*, (4), 1254-1259.
16. Bone, S. E.; Bargar, J. R.; Sposito, G., Mackinawite (FeS) Reduces Mercury(II) under Sulfidic Conditions. *Environmental Science & Technology* **2014,** *48*, (18), 10681-10689.
17. Wolfenden, S.; Charnock, J. M.; Hilton, J.; Livens, F. R.; Vaughan, D. J., Sulfide Species as a Sink for Mercury in Lake Sediments. *Environmental Science & Technology* **2005,** *39*, (17), 6644-6648.
18. Bailey, L. T.; Mitchell, C. P. J.; Engstrom, D. R.; Berndt, M. E.; Wasik, J. K. C.; Johnson, N. W., Influence of porewater sulfide on methylmercury production and partitioning in sulfate-impacted lake sediments. *Science of the Total Environment* **2017,** *580*, 1197-1204.
19. Gilmour, C. C.; Bullock, A. L.; McBurney, A.; Podar, M.; Elias, D. A., Robust Mercury Methylation across Diverse Methanogenic Archaea. *Mbio* **2018,** *9*, (2).
20. Gilmour, C. C.; Podar, M.; Bullock, A. L.; Graham, A. M.; Brown, S. D.; Somenahally, A. C.; Johs, A.; Hurt, R. A.; Bailey, K. L.; Elias, D. A., Mercury Methylation by Novel Microorganisms from New Environments. *Environmental Science & Technology* **2013,** *47*, (20), 11810-11820.

21. Fleming, E. J.; Mack, E. E.; Green, P. G.; Nelson, D. C., Mercury Methylation from Unexpected Sources: Molybdate-Inhibited Freshwater Sediments and an Iron-Reducing Bacterium. *Applied and Environmental Microbiology* **2006,** *72*, (1), 457.
22. Hamelin, S.; Amyot, M.; Barkay, T.; Wang, Y.; Planas, D., Methanogens: Principal Methylators of Mercury in Lake Periphyton. *Environmental Science & Technology* **2011,** *45*, (18), 7693-7700.
23. Kerin, E. J.; Gilmour, C. C.; Roden, E.; Suzuki, M. T.; Coates, J. D.; Mason, R. P., Mercury Methylation by Dissimilatory Iron-Reducing Bacteria. *Applied and Environmental Microbiology* **2006,** *72*, (12), 7919-7921.
24. Yu, R.-Q.; Reinfelder, J. R.; Hines, M. E.; Barkay, T., Mercury Methylation by the Methanogen *Methanospirillum hungatei*. *Applied and Environmental Microbiology* **2013,** *79*, (20), 6325.
25. Podar, M.; Gilmour, C. C.; Brandt, C. C.; Soren, A.; Brown, S. D.; Crable, B. R.; Palumbo, A. V.; Somenahally, A. C.; Elias, D. A., Global prevalence and distribution of genes and microorganisms involved in mercury methylation. *Science Advances* **2015,** *1*, (9).
26. Hsu-Kim, H.; Eckley, C. S.; Achá, D.; Feng, X.; Gilmour, C. C.; Jonsson, S.; Mitchell, C. P. J., Challenges and opportunities for managing aquatic mercury pollution in altered landscapes. *Ambio* **2018,** *47*, (2), 141-169.
27. Zhang, T.; Kim, B.; Levard, C.; Reinsch, B. C.; Lowry, G. V.; Deshusses, M. A.; Hsu-Kim, H., Methylation of Mercury by Bacteria Exposed to Dissolved, Nanoparticulate, and Microparticulate Mercuric Sulfides. *Environmental Science & Technology* **2012,** *46*, (13), 6950-6958.
28. Zhang, T.; Kucharzyk, K. H.; Kim, B.; Deshusses, M. A.; Hsu-Kim, H., Net Methylation of Mercury in Estuarine Sediment Microcosms Amended with Dissolved, Nanoparticulate, and Microparticulate Mercuric Sulfides. *Environmental Science & Technology* **2014,** *48*, (16), 9133-9141.
29. Pham, A. L.-T.; Morris, A.; Zhang, T.; Ticknor, J.; Levard, C.; Hsu-Kim, H., Precipitation of nanoscale mercuric sulfides in the presence of natural organic matter: Structural properties, aggregation, and biotransformation. *Geochimica et Cosmochimica Acta* **2014,** *133*, (0), 204-215.
30. Graham, A. M.; Aiken, G. R.; Gilmour, C. C., Dissolved Organic Matter Enhances Microbial Mercury Methylation Under Sulfidic Conditions. *Environmental Science & Technology* **2012,** *46*, (5), 2715-2723.
31. Jonsson, S.; Skyllberg, U.; Nilsson, M. B.; Westlund, P.-O.; Shchukarev, A.; Lundberg, E.; Björn, E., Mercury Methylation Rates for Geochemically Relevant HgII Species in Sediments. *Environmental Science & Technology* **2012,** *46*, (21), 11653-11659.
32. Jonsson, S.; Skyllberg, U.; Nilsson, M. B.; Lundberg, E.; Andersson, A.; Björn, E., Differentiated availability of geochemical mercury pools controls methylmercury levels in estuarine sediment and biota. *Nature Communications* **2014,** *5*, 4624.
33. Schartup, A. T.; Balcom, P. H.; Mason, R. P., Sediment-Porewater Partitioning, Total Sulfur, and Methylmercury Production in Estuaries. *Environmental Science & Technology* **2014,** *48*, (2), 954-960.
34. Marvin-DiPasquale, M.; Lutz, M. A.; Brigham, M. E.; Krabbenhoft, D. P.; Aiken, G. R.; Orem, W. H.; Hall, B. D., Mercury Cycling in Stream Ecosystems. 2. Benthic Methylmercury Production and Bed Sediment−Pore Water Partitioning. *Environmental Science & Technology* **2009,** *43*, (8), 2726-2732.

35. Moreau, J. W.; Gionfriddo, C. M.; Krabbenhoft, D. P.; Ogorek, J. M.; DeWild, J. F.; Aiken, G. R.; Roden, E. E., The Effect of Natural Organic Matter on Mercury Methylation by Desulfobulbus propionicus 1pr3. *Frontiers in Microbiology* **2015,** *6*, (1389).
36. Kelly, S.; Hesterberg, D.; Ravel, B., Analysis of soils and minerals using X-ray absorption spectroscopy. *Methods of soil analysis. Part* **2008,** *5*, 387-463.
37. Ravel, B.; Newville, M., ATHENA, ARTEMIS, HEPHAESTUS: data analysis for X-ray absorption spectroscopy using IFEFFIT. *Journal of Synchrotron Radiation* **2005,** *12*, (4), 537-541.
38. Avellan, A.; Stegemeier, J. P.; Gai, K.; Dale, J.; Hsu-Kim, H.; Levard, C.; O'Rear, D.; Hoelen, T. P.; Lowry, G. V., Speciation of Mercury in Selected Areas of the Petroleum Value Chain. *Environmental Science & Technology* **2018,** *52*, (3), 1655-1664.
39. Newville, M., IFEFFIT : interactive XAFS analysis and FEFF fitting. *Journal of Synchrotron Radiation* **2001,** *8*, (2), 322-324.
40. Gilmour, C. C.; Elias, D. A.; Kucken, A. M.; Brown, S. D.; Palumbo, A. V.; Schadt, C. W.; Wall, J. D., Sulfate-reducing bacterium Desulfovibrio desulfuricans ND132 as a model for understanding bacterial mercury methylation. *Applied Environmental Microbiology* **2011,** *77*, (12), 3938-51.
41. Benoit, J. M.; Gilmour, C. C.; Mason, R. P., Aspects of Bioavailability of Mercury for Methylation in Pure Cultures of *Desulfobulbus propionicus* (1pr3). *Applied and Environmental Microbiology* **2001,** *67*, (1), 51-58.
42. Hintelmann, H.; Evans, R. D., Application of stable isotopes in environmental tracer studies – Measurement of monomethylmercury (CH_3Hg^+) by isotope dilution ICP-MS and detection of species transformation. *Fresenius' Journal of Analytical Chemistry* **1997,** *358*, (3), 378-385.
43. Hintelmann, H.; Evans, R. D.; Villeneuve, J. Y., Measurement of mercury methylation in sediments by using enriched stable mercury isotopes combined with methylmercury determination by gas chromatography–inductively coupled plasma mass spectrometry. *Journal of Analytical Atomic Spectrometry* **1995,** *10*, (9), 619-624.
44. Stürup, S.; Chen, C.; Jukosky, J.; Folt, C., Isotope dilution quantification of $^{200}Hg^{2+}$ and $CH_3{}^{201}Hg^+$ enriched species-specific tracers in aquatic systems by cold vapor ICPMS and algebraic de-convoluting. *International Journal of Mass Spectrometry* **2005,** *242*, (2), 225-231.
45. EPA, US EPA Method 1630 for methylmercury analysis. **1998**.
46. Horvat, M.; Liang, L.; Bloom, N. S., Comparison of distillation with other current isolation methods for the determination of methyl mercury compounds in low level environmental samples: Part II. Water. *Analytica Chimica Acta* **1993,** *282*, (1), 153-168.
47. Ticknor, J. L.; Kucharzyk, K. H.; Porter, K. A.; Deshusses, M. A.; Hsu-Kim, H., Thiol-Based Selective Extraction Assay to Comparatively Assess Bioavailable Mercury in Sediments. *Environmental Engineering Science* **2015**.
48. Gill, G. A.; Fitzgerald, W. F., Picomolar mercury measurements in seawater and other materials using stannous chloride reduction and two-stage gold amalgamation with gas phase detection. *Marine Chemistry* **1987,** *20*, (3), 227-243.
49. Scherrer, P., Bestimmung der Grosse und der inneren Struktur von Kolloidteilchen mittels Rontgensrahlen [Determination of the size and internal structure of colloidal particles using X-rays]. *Nachr Ges Wiss Goettingen, Math-Phys Kl.* **1918,** *2*, 96-100.

50. Jeong, H. Y.; Lee, J. H.; Hayes, K. F., Characterization of synthetic nanocrystalline mackinawite: Crystal structure, particle size, and specific surface area. *Geochimica et Cosmochimica Acta* **2008,** *72*, (2), 493-505.
51. O'Day, P. A.; Rivera, N., Jr.; Root, R.; Carroll, S. A., X-ray absorption spectroscopic study of Fe reference compounds for the analysis of natural sediments. *American Mineralogist* **2004,** *89*, (4), 572-585.
52. Frueh, A. J., Jnr; Gray, N., Confirmation and refinement of the structure of $Hg_3S_2Cl_2$. *Acta Crystallographica Section B* **1968,** *24*, (1), 156-157.
53. Poulin, B. A.; Aiken, G. R.; Nagy, K. L.; Manceau, A.; Krabbenhoft, D. P.; Ryan, J. N., Mercury transformation and release differs with depth and time in a contaminated riparian soil during simulated flooding. *Geochimica Et Cosmochimica Acta* **2016,** *176*, 118-138.
54. Wiatrowski, H. A.; Das, S.; Kukkadapu, R.; Ilton, E. S.; Barkay, T.; Yee, N., Reduction of Hg(II) to Hg(0) by Magnetite. *Environmental Science & Technology* **2009,** *43*, (14), 5307-5313.
55. Gerbig, C. A.; Kim, C. S.; Stegemeier, J. P.; Ryan, J. N.; Aiken, G. R., Formation of Nanocolloidal Metacinnabar in Mercury-DOM-Sulfide Systems. *Environmental Science & Technology* **2011,** *45*, (21), 9180-9187.
56. Poulin, B. A.; Gerbig, C. A.; Kim, C. S.; Stegemeier, J. P.; Ryan, J. N.; Aiken, G. R., Effects of Sulfide Concentration and Dissolved Organic Matter Characteristics on the Structure of Nanocolloidal Metacinnabar. *Environmental Science & Technology* **2017,** *51*, (22), 13133-13142.
57. GreffiÉ, C.; Parron, C.; Amouric, M., HRTEM study of freeze-dried and untreated synthetic ferrihydrites: consequences of sample processing. *Clay Minerals* **2001,** *36*, (3), 381-387.
58. Xia, K.; Skyllberg, U. L.; Bleam, W. F.; Bloom, P. R.; Nater, E. A.; Helmke, P. A., X-ray Absorption Spectroscopic Evidence for the Complexation of Hg(II) by Reduced Sulfur in Soil Humic Substances. *Environmental Science & Technology* **1999,** *33*, (2), 257-261.
59. Nagy, K. L.; Manceau, A.; Gasper, J. D.; Ryan, J. N.; Aiken, G. R., Metallothionein-Like Multinuclear Clusters of Mercury(II) and Sulfur in Peat. *Environmental Science & Technology* **2011,** *45*, (17), 7298-7306.
60. Skyllberg, U.; Bloom, P. R.; Qian, J.; Lin, C.-M.; Bleam, W. F., Complexation of Mercury(II) in Soil Organic Matter: EXAFS Evidence for Linear Two-Coordination with Reduced Sulfur Groups. *Environmental Science & Technology* **2006,** *40*, (13), 4174-4180.
61. Ndu, U.; Christensen, G. A.; Rivera, N. A.; Gionfriddo, C. M.; Deshusses, M. A.; Elias, D. A.; Hsu-Kim, H., Quantification of Mercury Bioavailability for Methylation Using Diffusive Gradient in Thin-Film Samplers. *Environmental Science & Technology* **2018,** *52*, (15), 8521-8529.
62. Hellal, J.; Burnol, A.; Locatelli, A.; Battaglia-Brunet, F., Experimental Column Setup for Studying Anaerobic Biogeochemical Interactions Between Iron (Oxy) Hydroxides, Trace Elements, and Bacteria. *Jove-Journal of Visualized Experiments* **2017**, (130).
63. Mehrotra, A. S.; Horne, A. J.; Sedlak, D. L., Reduction of Net Mercury Methylation by Iron in Desulfobulbus propionicus (1pr3) Cultures: Implications for Engineered Wetlands. *Environmental Science & Technology* **2003,** *37*, (13), 3018-3023.
64. Mehrotra, A. S.; Sedlak, D. L., Decrease in Net Mercury Methylation Rates Following Iron Amendment to Anoxic Wetland Sediment Slurries. *Environmental Science & Technology* **2005,** *39*, (8), 2564-2570.

65. Ulrich, P. D.; Sedlak, D. L., Impact of Iron Amendment on Net Methylmercury Export from Tidal Wetland Microcosms. *Environmental Science & Technology* **2010,** *44*, (19), 7659-7665.